Monte Carlo simulations of the nucleation and growth process of colloidal particles

Chia-Yi Yang, Wan Y. Shih, and Wei-Heng Shih
Department of Materials Engineering, Drexel University, Philadelphia, Pennsylvania 19104
(Received 12 May 2000; published 19 July 2001)

We have examined the effect of the total initial monomer concentration and that of the monomer-monomer attraction energy on the nucleation and growth process of colloidal particles using a reversible aggregation model (Shih-Aksay-Kikuchi model) with the Monte Carlo method. We showed that the equilibrium monomer concentration c_e exhibited a peak with respect to the total initial monomer concentration c_t. Furthermore, the solution may be divided into three regimes with respect to c_t. In the first regime where the initial monomer concentration was low, all monomers remained as individual monomers in the solution and c_e increased linearly with c_t. In the second regime where small clusters of monomers began to form, c_e underwent a peak with respect to c_t. In the third regime where large particles form, c_e slowly decreased with c_t. Moreover, with increasing monomer-monomer attraction energy, the peak in c_e moved to a lower c_t and became sharper. The equilibrium monomer concentration surrounding a particle with respect to particle size was shown to agree with the Kelvin equation, indicating that the model can indeed capture the equilibrium solution physics involving colloidal particles. The peak exhibited in c_e versus c_t was manifested as a peak in the monomer concentration versus time under conditions where monomers were gradually fed to the solution. The present simulation is a simulation model for illustrating a peaked solute concentration with respect to time first proposed by LaMer and Dinegar. We further showed that the supersaturation peak in the monomer concentration versus time depended on the feeding rate. The peak height increased with an increasing feeding rate.

DOI: 10.1103/PhysRevE.64.021403 PACS number(s): 82.70.Dd, 83.80.Hj, 81.10.Dn, 64.60.Qb

I. INTRODUCTION

The widely accepted view of nucleation and growth of monodispersed colloidal particles in suspensions was first proposed by LaMer and Dinegar [1]. In their study of formation of monodispersed sulfur hydrosols by slow decomposition of dilute sodium thiosulfate in dilute hydrochloric acid, they observed the formation of monodispersed sulfur sols by spontaneous nucleation upon supersaturation followed by growth of particles. Because the decomposition of sodium thiosulfate slowly released molecular sulfur in the solution, they proposed that the sulfur concentration in the solution with respect to time underwent three stages as shown in Fig. 1. In the early stage, i.e., stage I, the sulfur concentration increased with time until the solution is supersaturated (stage II) where rapid nucleation occurred that reduced the degree of supersaturation and the sulfur concentration exhibited a maximum. After the rapid nucleation stage, particles grew by molecular addition (stage III). During stage III, the sulfur concentration continued to decrease and eventually leveled off. While the idea of LaMer and Dinegar as outlined in Fig. 1 has been widely accepted, the notion that particles grow by molecular addition after the nuclei are formed was later challenged by numerous experimental observations that evidenced aggregation during growth of particles [2–6]. To account for the aggregation aspect during particle growth, Bogush and Zukoski [7] developed an aggregative growth model for the formation of colloidal silica particles [8] by incorporating the interparticle Derjaguin-Landau-Verwey-Overbeek [7] interaction in the Smoluchowski aggregation equation. With the binary aggregation rate modified by the interparticle repulsion that increased with aggregate size, they were able to obtain a finite cluster size that grew with time. Although Bogush and Zukoski's aggregative growth model highlighted the aggregative aspect of colloidal particle growth, the aggregation process in their model was irreversible. Once an aggregate was formed its size could not be reduced. Furthermore, there was no dissolution mechanism to allow aggregates to equilibrate with the surrounding solution nor could an irreversible aggregative model account for the fact that the silica particles formed were spherical that required substantial restructuring in the aggregates. It is generally accepted that during the nucleation stage, embryos constantly form and dissolve. It is important that a model not only allows aggregation but also dissolution. As far as we know, there have been no microscopic simulation models that predict the peaked solute concentration versus time pro-

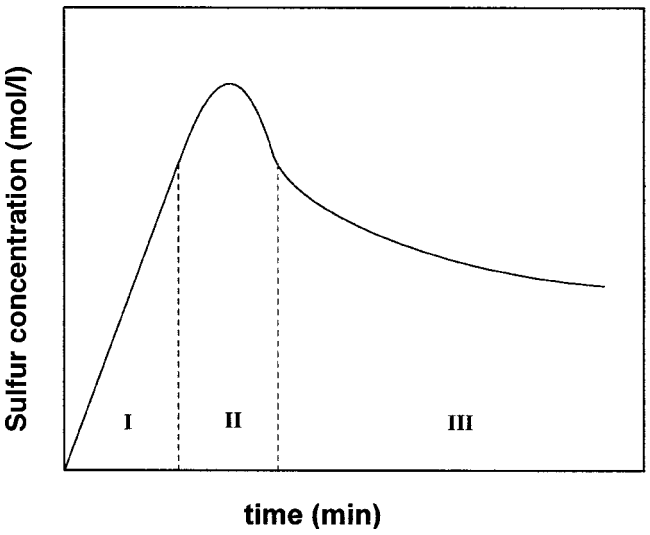

FIG. 1. A schematic of the sulfur concentration versus time replotted from Ref. [1].

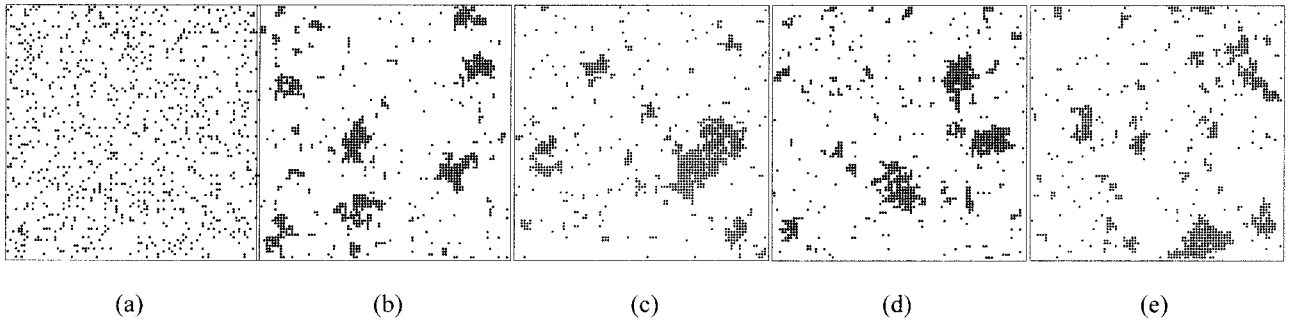

FIG. 2. Temporal evolution of a solution starting with randomly distributed monomers in a 90×90 cell with $c_t=0.111$, $E=2k_BT$ at (a) $t=0\tau$, (b) 5000τ, (c) $80\,000\tau$, (d) $120\,000\tau$, and (e) $160\,000\tau$.

posed by LaMer and Dinegar. Nor have there been microscopic nucleation and growth models that address both aggregation and dissolution simultaneously.

The purpose of this paper is to simulate with a Monte Carlo method the nucleation and growth process of colloidal particles using a reversible aggregation model that allows aggregation, dissolution, and restructuring of aggregates to occur. Specifically, we would like to examine the nucleation and growth processes at various concentrations and energetic conditions, and compare the solute concentration versus time with that proposed by LaMer and Dinegar. The model we used is the Shih-Aksay-Kikuchi (SAK) model [9,10] which was initially developed to describe colloidal aggregates formed with finite interparticle attraction energies [10,11]. The model allowed colloidal particles and clusters to aggregate via the cluster-cluster aggregation mechanism [12,13] while taking into account the effect of a finite interparticle attraction energy that allowed particles to unbind from a cluster. The combination of the aggregation feature and the finite interparticle interactions enabled the model to simulate a wide range of colloidal phenomena from aggregation, dispersion, to microphase separation. In earlier work, the model was used to study the effect of finite interparticle attraction energy on the fractal dimension of colloidal aggregates [9–11], and to study the effect of restructuring on the structure of particulate networks [14,15]. Later, the model was extended to study the stability of binary colloidal suspensions with depletion flocculation and depletion restabilization [16,17], and heterogeneous aggregation [18]. Although nucleation and growth have long been regarded as a thermodynamically driven phenomenon, experiments revealed that aggregation occurred at least in the early stage of particle growth [2–7]. A model such as the SAK model that allows both aggregation and relaxation by energetic considerations can simulate both particle formation and dissolution, and hence give a more accurate picture of the nucleation and growth process in colloidal suspensions.

II. MODEL

As discussed above, the formation of colloidal particles involves aggregation. In what follows, we will refer to the precipitating units that aggregate to form colloidal particles as ''monomers'' that appear as dots in all figures. We refer to the resultant clusters as ''clusters'' or ''particles'' that often appear as compact rounded clusters. We may use the terms ''clusters,'' ''particles,'' or ''colloidal particles'' interchangeably. In principle, the monomers, i.e., the precipitating units that aggregate to form colloidal particles may represent the individual molecules or atoms. However, this would require a large number of monomers that is beyond the present simulation capability. For practicality, the monomers represent microscopic or mesoscopic clusters of atoms or molecules that further aggregate to form colloidal particles. The simulations were done in two dimensions on a square lattice. For convenience, we took the lattice constant of the underlying square lattice as unity. As we will show below, the two-dimensional simulations were sufficient to illustrate the physics involved.

Initially, N monomers were randomly distributed in an

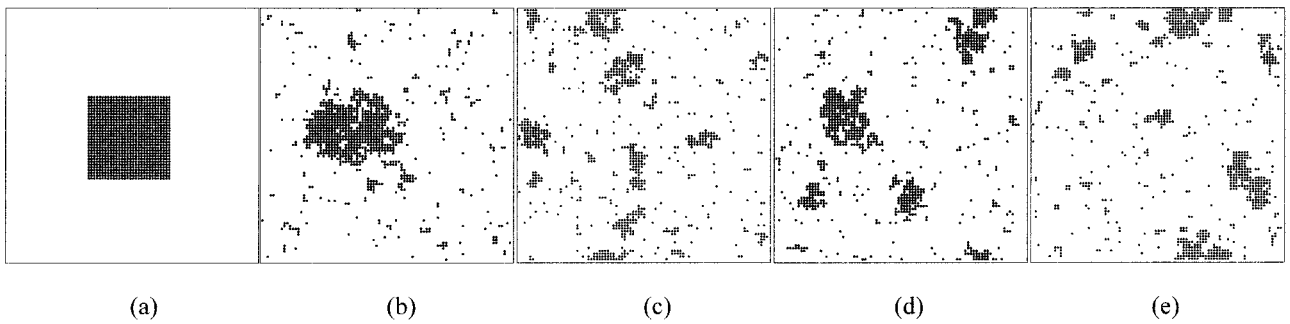

FIG. 3. Temporal evolution of a solution starting with a square block of monomers in the center of a 90×90 cell with $c_t=0.111$, $E=2k_BT$ at (a) $t=0\tau$, (b) 5000τ, (c) $80\,000\tau$, (d) $120\,000\tau$, and (e) $160\,000\tau$.

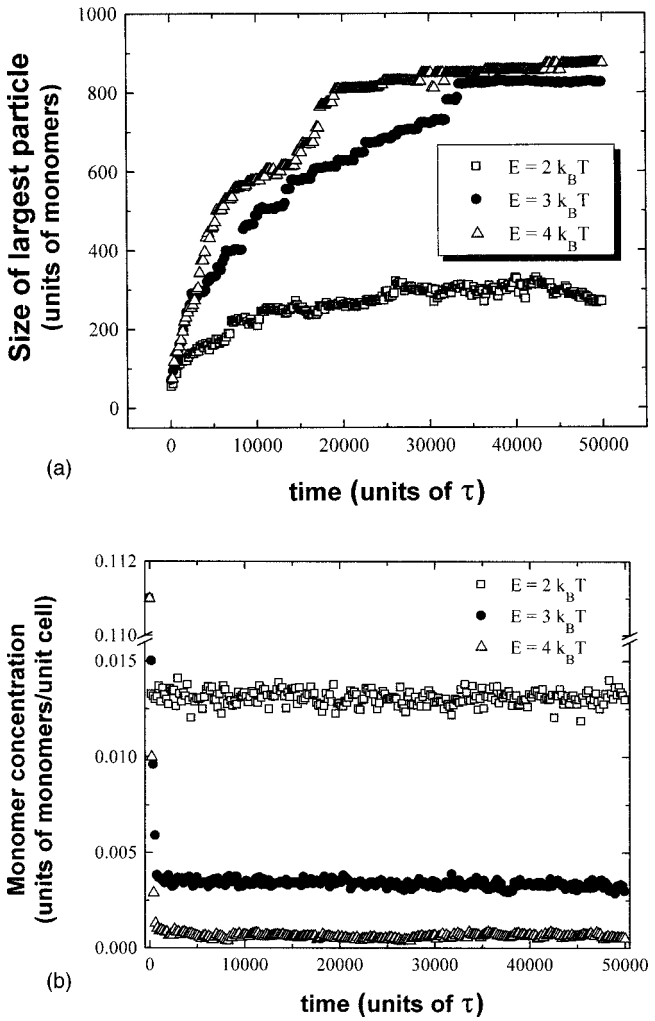

FIG. 4. (a) The size of the biggest particle versus time, and (b) the monomer concentration versus time at $c_t=0.111$ in a 90×90 cell with $E=2k_BT$, $3k_BT$, and $4k_BT$. The data points were obtained by averaging over 20 independent runs.

$L_x\times L_y$ lattice. The total initial monomer concentration is, therefore, $c_t=N/(L_xL_y)$. After a time interval τ_D each monomer moved to one of its empty neighboring sites randomly to simulate diffusion. When a monomer moved next to another monomer or cluster, they formed a bigger cluster. Meanwhile, clusters could also perform random walk as a whole. For a cluster of m monomers, it attempted to move as a whole by one lattice constant in one of the four directions at random after each time interval $m^{-1/2}\tau_D$. The $m^{-1/2}\tau_D$ stepping time for a cluster of m monomers in two dimensions is chosen according to the Einstein relation that the diffusion coefficient is inversely proportional to the radius of the particles. When a cluster was next to other clusters or monomers, they formed a bigger cluster. This cluster-cluster aggregation mechanism has been proven the prevalent aggregation mechanism that governed the fractal dimension of colloidal aggregates formed under highly attractive conditions [19]. Meanwhile, between monomers, we considered a nearest-neighbor finite attraction energy, $-E$. Because E was finite, the bonds between a monomer and its neighbors

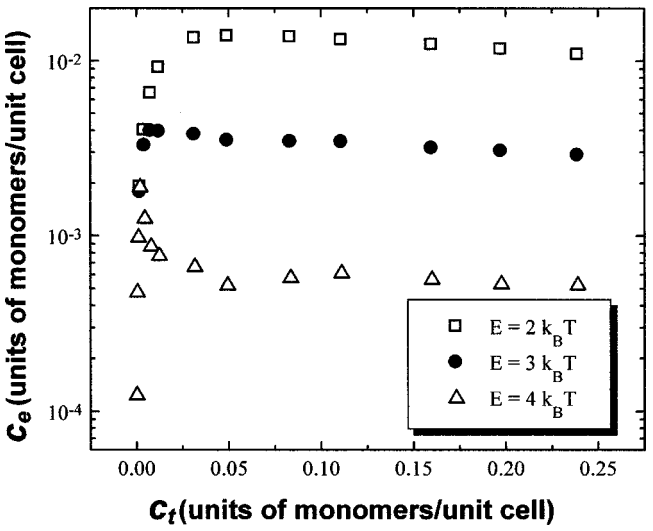

FIG. 5. The equilibrium monomer concentration c_e versus the total monomer concentration c_t in a 90×90 cell with $E=2k_BT$, $3k_BT$, and $4k_BT$. The data points were obtained by averaging over the time period $(50\,000–200\,000)\tau$ of three independent runs.

within a cluster could break by thermal agitation. The probability for a monomer to break the bonds with its neighbors and move to one of its unoccupied neighboring sites at random was determined by the Boltzmann factor $(1/\tau_R)e^{-\Delta E/k_BT}$ where ΔE was the change in energy due to the move and $1/\tau_R$ is the unbinding attempt frequency. Note that with a square underlying lattice, a monomer surrounded by four neighbors within a cluster could not break up with its neighbors because it did not have an unoccupied neighboring site to move to after the breakup. Although the model is a discrete one, the consideration of the breakup of individual monomers within a cluster permitted densification of clusters as well as dissolution. The former involved movements of monomers within a cluster to other parts of the cluster and the latter involved movements of monomers within a cluster into the solution. As we will show below, the intermonomer attraction energy $-E$ is related to the monomer solubility. A large (small) E corresponds to a small (large) solubility. For example, many oxides, e.g., boehmite (AlOOH) become more soluble in acidic conditions [20]. Therefore, for such oxides, lowering the pH is equivalent to decreasing E. At present, we did not consider the interaction energy between clusters. As indicated by the aggregative growth model [7] large repulsion energy between large particles can prevent further aggregation between large particles. In the present study, we focused on the effects of monomer attraction energy (i.e., solubility) and initial total monomer concentration on the nucleation and growth process. Effects of intercluster interactions will be studied in a separate publication.

During the simulations, the top and the bottom of the simulation cell were connected by the periodic boundary conditions. The left and right sides of the simulation cell were hard walls, i.e., walls that were noninteractive to the monomers and clusters except that they were impenetrable to the monomers and clusters. The mixed boundary conditions used here were designed for future study of the coating of precipitating species on a flat surface. Care has been taken to

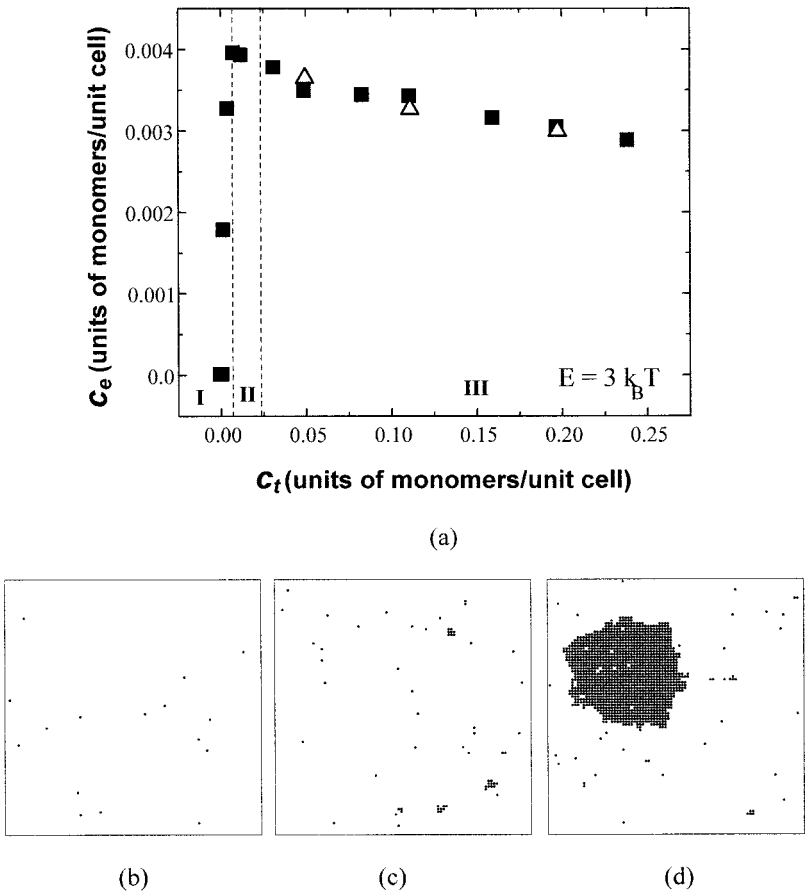

FIG. 6. (a) c_e versus c_t, (b) a snapshot in regime I at $c_t=0.002$, (c) a snapshot in regime II at $c_t=0.008$, and (d) a snapshot in regime III at $c_t=0.16$ for $E=3k_BT$. All the snapshots were taken under the equilibrium condition at $t=200\,000\tau$ in a 90×90 simulation cell. Also shown in (a) were the results obtained from simulations cells with periodic boundary conditions (open triangles) in both x and y directions. In (a), the results obtained both with the mixed boundary conditions and with periodic boundary conditions collapse on one curve, indicating that the present simulation cell was large enough that the mixed boundary conditions did not affect the results.

make sure that the simulation cell was large enough and that the hard-wall boundary conditions in the x direction did not affect the results [see Figs. 6(a) and 8(a)]. Note that in principle, the time constant τ_D for diffusion and the time constant τ_R for the unbinding process could be different. For convenience, we chose $\tau_D=\tau_R=\tau$, i.e., after every time interval τ every monomer in the solution attempted random walk once and every monomer in a cluster (particle) attempted to unbind once.

III. RESULTS

To examine the nucleation and growth process, we started with N monomers in an $L\times L$ simulation cell, i.e., the total monomer concentration $c_t=N/L^2$. Note that most of the simulations were performed on a 90×90 cell except for very low c_t's where we must use larger cells in order to have enough monomers in the cell. We allowed the simulations to run for a long time until the solutions reached equilibrium, by which we mean the final monomer concentration and cluster size (or particle size) remained unchanged. Figure 2 shows temporal evolution of a solution of $c_t=0.111$ at $t=0\tau$ (a), 5000τ (b), $80\,000\tau$ (c), $120\,000\tau$ (d), and $160\,000\tau$ (e). Notice that the snapshots shown in Figs. 2(d) and 2(e) are more or less the same, indicating that the solution had reached the equilibrium condition by $t=120\,000\tau$. To further ensure that we have reached equilibrium in the simulations, we started simulations with monomers initially put in a square block at the center of the cell as shown in Fig. 3(a). Figure 3(a) has the same c_t and the same attraction energy as Fig. 2(a). The subsequent temporal evolution shown in Figs. 3(a)–3(e), snapshots taken $t=0\tau$ (a), 5000τ (b), $80\,000\tau$ (c), $120\,000\tau$ (d), and $160\,000\tau$ (e), vividly illustrate the dissolution process. First the square block became rounded as monomers dissolved into the solution [Fig. 3(b)]. As more monomers went into the solution smaller clusters formed [Fig. 3(c)]. Eventually, the clusters reached an equilibrium size [Figs. 3(d) and 3(e)]. The solution shown in Figs. 2(a)–2(e) had the same total number of monomers and the same monomer attraction energy as that shown in Figs. 3(a)–3(e). By comparing Figs. 2(d)–2(e) and Figs. 3(d)–3(e), one may conclude that regardless of the difference in the initial configurations, the two solutions reached the same final configurations. This further indicates that the present reversible aggregation model is indeed capable of reaching equilibrium conditions. In Figs. 4(a) and 4(b), we respectively show the biggest particle size (or the biggest cluster size) versus time and the monomer concentration versus time of a solution of $c_t=0.111$ with $E=2k_BT$, $3k_BT$, and $4k_BT$. The data points shown in Figs. 4(a) and 4(b) were averaged over 20 independent runs. It is clear that both the particle sizes and the monomer concentrations reached equilibrium values. The equilibrium particle size was smaller and the equilibrium monomer concentration higher with decreased E. Particle size also increased more slowly with decreased E.

In Fig. 5, we show the equilibrium monomer concentration c_e versus the total monomer concentration c_t for $E=2k_BT$, and $3k_BT$, and $4k_BT$. The data points shown in Fig.

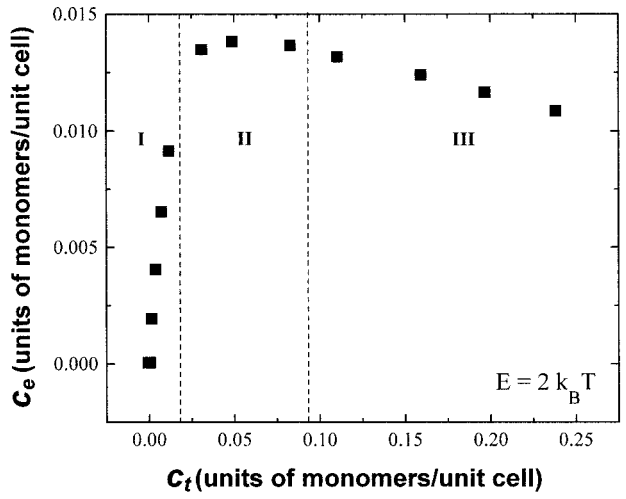

(a)

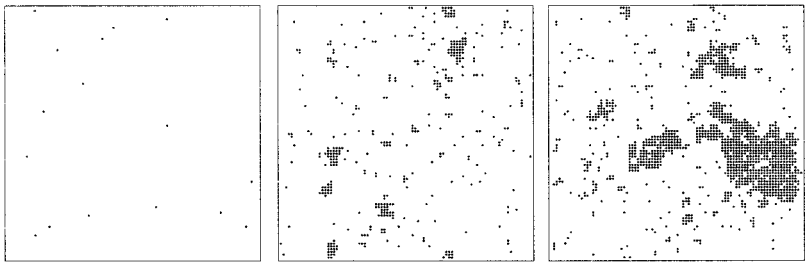

(b) (c) (d)

FIG. 7. (a) c_e versus c_t, (b) a snapshot in regime I at $c_t=0.002$, (c) a snapshot in regime II at $c_t=0.05$, and (d) snapshot in regime III at $c_t=0.16$ for $E=2k_BT$. All the snapshots were taken under the equilibrium condition at $t=200\,000\tau$ in a 90×90 simulation cell.

5 were obtained by averaging over the time period $(50\,000–200\,000)\tau$ of three independent runs. Notice that the equilibrium monomer concentration exhibited a peak with respect to the total monomer concentration. Moreover, the peak became more prominent with increasing E and the peak also moved to a lower c_t.

For a given c_t, we also performed simulations by initially putting all the monomers in the square block at the center of the cell similar to what was shown in Fig. 3(a) and allowed the system to equilibrate. The equilibrium monomer concentration c_e versus c_t obtained from such dissolution simulations were the same as those shown in Fig. 5. The final equilibrium snapshots obtained from dissolution simulations were also similar to those formed from initial solutions. Examination of the final equilibrium snapshots revealed that each of the three curves shown in Fig. 5 might be divided into three regimes. Figure 6(a) is the c_e versus c_t for $E=3k_BT$ shown in Fig. 5 and the three regimes are marked with I, II, and III. Typical equilibrium snapshots at $t=200\,000\tau$ obtained in regimes I, II, and III are shown in Figs. 6(b)–6(d), respectively. Figure 6(b) obtained at $c_t=0.002$ in regime I shows that most of the monomers remained as individual monomers in regime I. The equilibrium monomer concentration c_e was linear with c_t (not shown), indicating the solution is below the solubility limit. Figure 6(c) obtained in regime II at $c_t=0.008$ shows that in regime II small clusters emerged, indicating that the solution was above the solubility limit (i.e., supersaturated). Meanwhile, the small clusters shown in Fig. 6(c) were unstable; they constantly changed shape, dissolved, and reformed as expected of the nucleation stage. Figure 6(d) obtained in regime III at $c_t=0.16$ shows that a big rounded particle was in equilibrium with monomers and small clusters in the solutions.

For comparison, Fig. 7(a) shows the three regimes in the c_e versus c_t for $E=2k_BT$ and Figs. 7(b)–(d), respectively, show the corresponding equilibrium snapshots obtained in regimes I, II, and III obtained at $t=200\,000\tau$. Compared to Figs. 6(a)–(d), the solutions with $E=2k_BT$ had a higher solubility limit. Therefore, regime II occurred at higher concentrations [Fig. 7(a)]. The size of the small clusters shown in Fig. 7(c) was also larger than that of those shown in Fig. 6(c). In regime III [Fig. 7(d)], the solution consisted of individual monomers, small clusters, and larger clusters of various sizes. The higher solubility at $E=2k_BT$ is apparent when comparing Figs. 7(c)–(d) to Figs. 6(c)–(d).

Figure 8(a) shows the three regimes in the c_e versus c_t plot for $E=4k_BT$ and Figs. 8(b)–(d) show the equilibrium snapshots obtained at $t=200\,000\tau$ in regimes I, II, and III, respectively. Compared to solutions with $E=2k_BT$ and $3k_BT$, the solutions with $E=4k_BT$ exhibited a lower solubility limit and small clusters began to appear at a lower c_t [Fig. 8(a)]. Note that the cell size of Fig. 8(b) was 180×180, four times larger than that of Figs. 8(c) and 8(d), which was 90×90. Because the solubility was much lower at $E=4k_BT$, it was necessary to have larger cells to obtain solutions in regime I. Therefore, the higher number of indi-

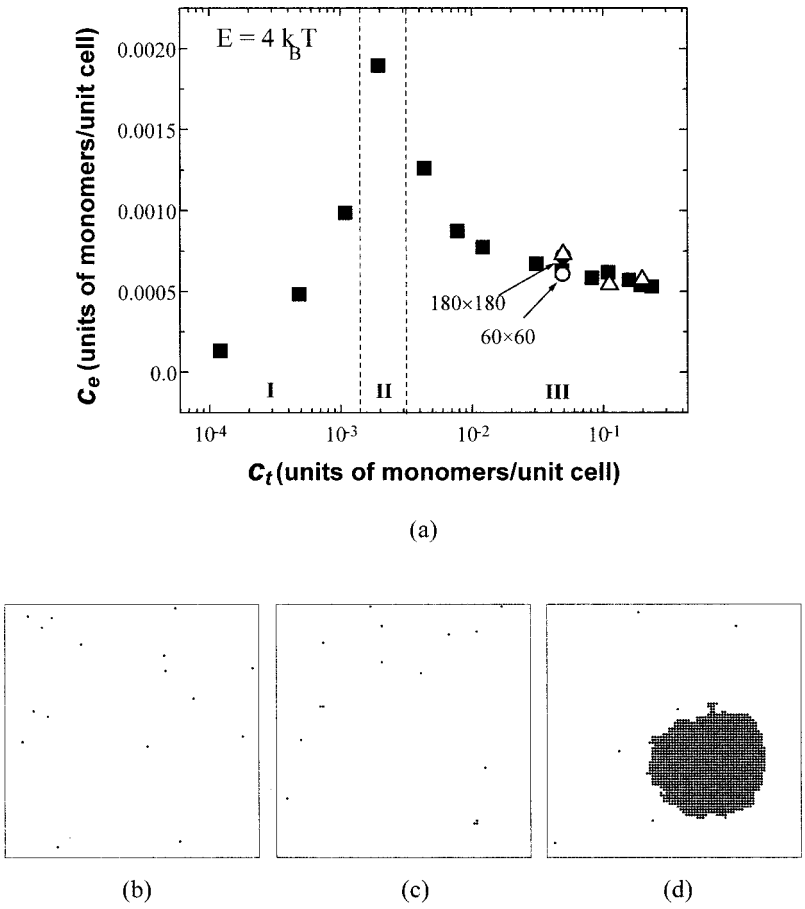

FIG. 8. (a) c_e versus c_t, (b) a snapshot in regime I at $c_t=2\times10^{-4}$ obtained in a 180×180 simulation cell, (c) a snapshot in regime II at $c_t=0.002$ obtained in a 90×90 simulation cell, and (d) a snapshot in regime III at $c_t=0.16$ obtained in a 90×90 simulation cell for $E=4k_BT$. All the snapshots were taken under the equilibrium condition at $t=200\,000\tau$. Also shown in (a) were the results obtained from simulations cells with periodic boundary conditions (open triangles) in both x and y directions and from different simulation cell sizes, 180×180 (filled circle) and 60×60 (open circle). The results obtained with the mixed boundary conditions, with periodic boundary conditions, and with different cell sizes all collapse on one curve, indicating that the present simulation cell was large enough that the mixed boundary conditions did not affect the results.

vidual monomers in Fig. 8(b) does not imply a higher monomer concentration because the actual cell size was larger. Instead, the actual monomer concentrations were as indicated in Fig. 8(a).

To make sure that the simulation cell size and the boundary conditions are adequate, we also included some results from larger simulation cells and from cells with periodic boundary conditions in the c_e versus c_t plot in both Figs. 6(a) and 8(a) at higher total monomer concentrations where inadequate cell sizes and the mixed boundary conditions could give different results. In both Figs. 6(a) and 8(a), the open triangles were results from simulations with the same cell size but with periodic boundary conditions. In Fig. 8(a), at $c_t=0.045$, results from simulation cells of 60×60 and 180×180 were also shown for comparison. Clearly, larger cell sizes and periodic boundary conditions did not give different equilibrium monomer concentrations, indicating that indeed the cell size we chose was large enough that neither the hard walls nor the cell size affected the results.

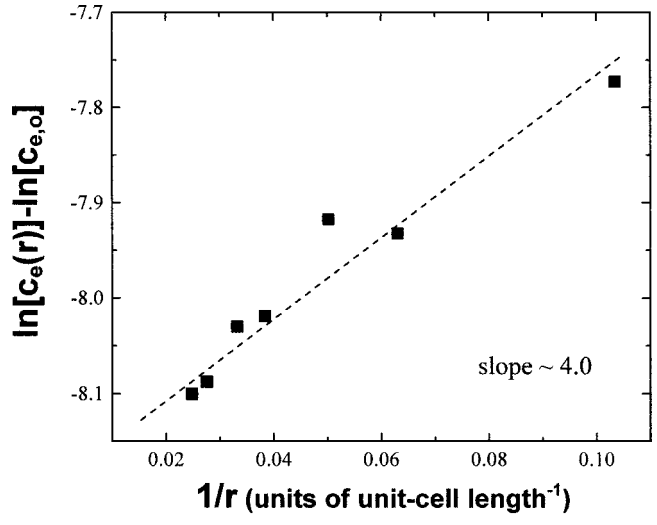

FIG. 9. $\ln[c_e(r)]-\ln[c_{e,o}]$ versus $1/r$ for $E=4k_BT$, where $c_{e,o}$ is the bulk equilibrium monomer concentration and r is the radius of the particles as defined in the text. The data points were obtained by averaging over the time period $(50\,000-200\,000)\tau$ of three independent runs.

Notice that in regime II, the size of the smaller clusters shown in Fig. 8(c) was smaller than those shown in Fig. 6(c) for $E=3k_BT$ and in Fig. 7(c) for $E=2k_BT$. Meanwhile, notice that in Fig. 8(d), the solution was dominated by one big round particle (cluster) in equilibrium with a few individual monomers. Notably, there were no smaller clusters. Under such conditions, the equilibrium monomer concentration may be related to the size of the dominant particle (cluster) in the cell and that the slow decrease of the equilibrium monomer concentration with an increasing c_t may be a result of the increased size of the dominant particle.

According to the Kelvin equation the equilibrium concentration $c_e(r)$ of a solution containing particles of radius r is related to r as

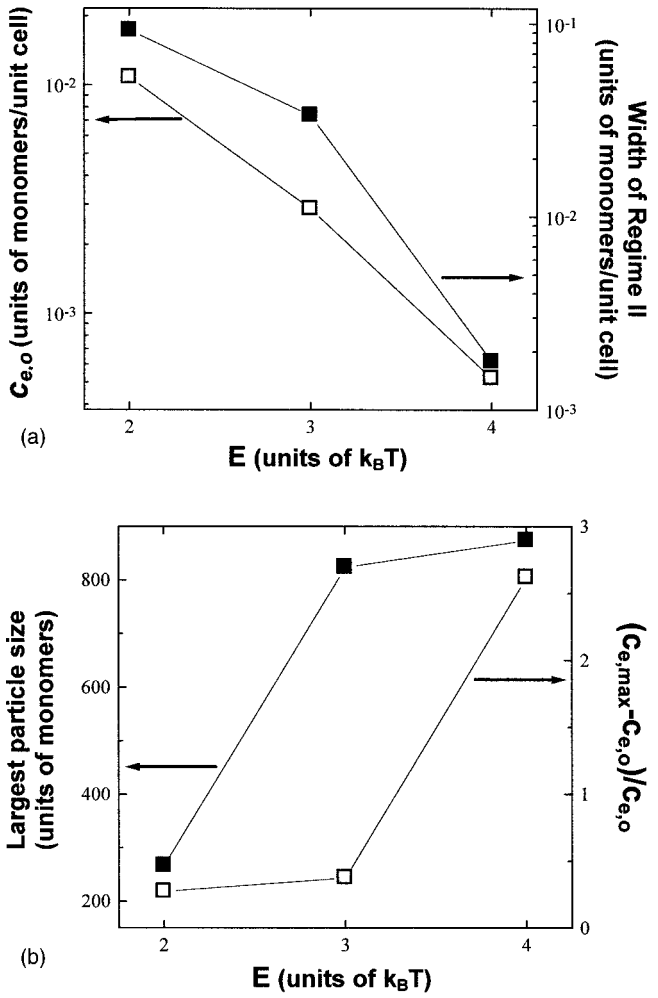

FIG. 10. (a) $c_{e,o}$ and width of region II versus E, (b) $(c_{e,\max}-c_{e,o})/c_{e,o}$ and largest particle size versus E where $c_{e,o}$ is the bulk saturation monomer concentration taken as the solubility, $c_{e,\max}$ is the peak equilibrium in region II, $(c_{e,\max}-c_{e,o})/c_{e,o}$ represents the degree of supersaturation, and the width of region II is as defined in the text.

$$\frac{c_e(r)}{c_{e,o}} = \exp\left(\frac{2\sigma}{k_BT}\frac{1}{r}\right)$$

where $c_{e,o}$ is the equilibrium bulk solution concentration, σ the surface tension of a flat interface between the solid and the solvent. To examine this, in Fig. 9 we plot $\ln[c_e(r)] - \ln[c_{e,o}]$ versus $1/r$ where $c_{e,o}$ was approximated as the equilibrium monomer concentration with the largest particles, and r was approximated as $r \cong \sqrt{N_p}/2$ with N_p being the number of monomers contained in the particle. The data points shown in Fig. 9 were obtained by averaging over the time period $(50\,000–200\,000)\tau$ of three independent runs. If the solution was truly dominated by one big particle and the Kelvin effect was at work, the plot in Fig. 9 should be linear with a slope equal to $2\sigma/k_BT$. With the square underlying lattice whose lattice constant being unity, the surface energy of a flat solid-solvent interface is $E/2$ at 0 K. For $E = 4k_BT$, the 0 K surface energy is thus $2k_BT$. While the surface tension σ at temperature T was not exactly the same

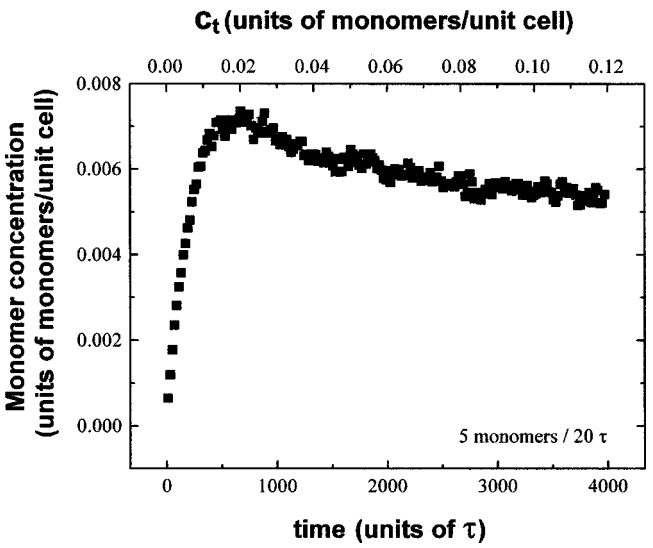

FIG. 11. The monomer concentration versus time with a monomer feeding rate of 5 monomers per 20τ. The final total monomer concentration was 0.123. All the data points were obtained by averaging 20 independent runs with $E = 3k_BT$ in a 90×90 simulation cell.

as the surface energy at 0 K, it was reasonable to expect σ to be close to the 0 K surface energy [21], which is $2k_BT$ in the present case. Thus, $2\sigma/k_BT$ is expected to be about 4. In Fig. 9, $\ln[c_e(r)] - \ln[c_{e,o}]$ versus $1/r$ was indeed linear with a slope about 4, indicating that the solution with $E = 4k_BT$ was dominated by one big particle and the slow decease in the equilibrium monomer concentration with respect to c_t was a manifestation of the Kelvin effect as a result of the increased size of the dominant particle with an increasing c_t in regime III of $E = 4k_BT$. This further illustrates that the present reversible aggregation model not only has the aggregation feature observed in many nucleation and growth studies but also is capable of displaying various equilibrium phenomena.

In regimes III of $E = 3k_BT$ and $E = 2k_BT$ [see Figs. 6(d) and 7(d)], in addition to the dominant particle (or cluster), smaller clusters also existed in the solution. This is especially apparent in the snapshot shown in Fig. 7(d) for $E = 2k_BT$. Unlike regime III of $E = 4k_BT$, particles of various sizes coexist in regime III of $E = 2k_BT$ and $3k_BT$. More than one particle size can contribute to enhance the equilibrium monomer concentration. Consequently, unlike that in regime III of $E = 4k_BT$, the equilibrium monomer concentration cannot be fitted to a dominant particle size in regime III of $E = 2k_BT$ and $3k_BT$.

For a given E, the solubility may be approximated as $c_{e,o}$, the saturated equilibrium monomer concentration at the highest $c_{\rm tot}$ and the degree of supersaturation may be defined as $(c_{e,\max}-c_{e,o})/c_{e,o}$ where $c_{e,\max}$ is the peak monomer concentration in region II. The width of region II may be defined as the width between the two total concentrations where c_e is half of $c_{e,\max}$. To summarize the effect of E on the solubility, the degree of supersaturation, the width of region II, and particle size, we plot $c_{e,o}$ and width of region II versus E in a semilogarithmic plot in Fig. 10(a), and $(c_{e,\max}-c_{e,\max})/c_{e,o}$ and largest particle size versus E in Fig. 10(b). It can be seen

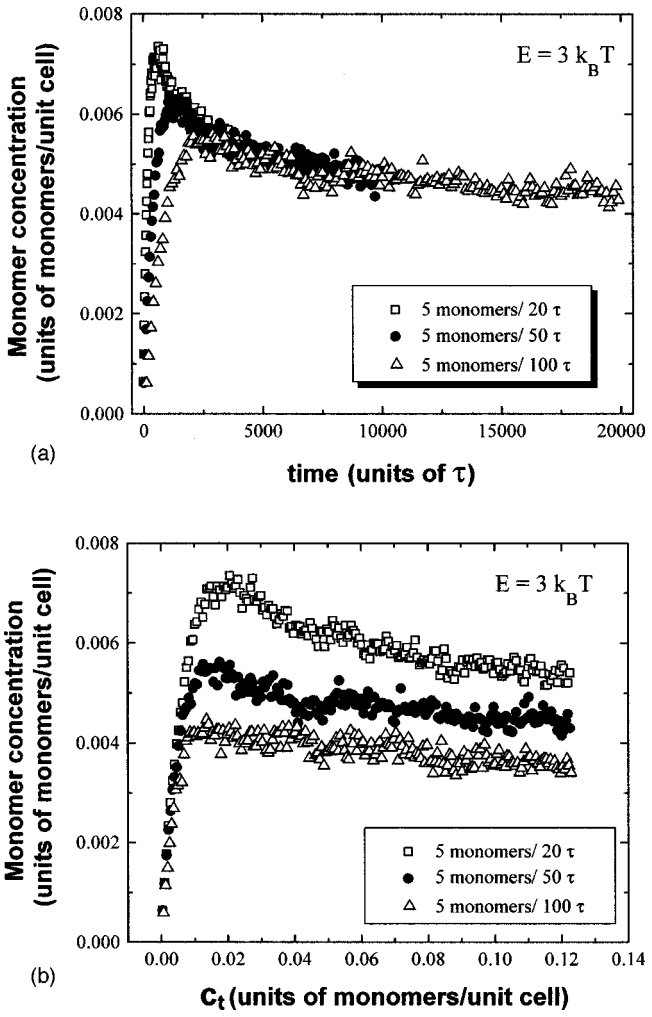

FIG. 12. (a) The monomer concentration versus time, and (b) the monomer concentration versus the corresponding c_t for various monomer feeding rates with $E=3k_BT$. All the data points were obtained by averaging over 20 independent runs.

that the solubility decreases roughly exponentially with an increasing E. Meanwhile, as the solubility decreases with an increasing E, so does the width of region II. On the other hand, Fig. 10(b) shows that the degree of supersaturation increases with an increasing E and the largest particle size also increases with an increasing E.

Note that a peaked c_e with respect to c_t looks similar that of the sulfur concentration versus time schematically shown in Fig. 1. In the sulfur hydrosols, molecular sulfur was derived by the decomposition of sodium thiosulfate. The total sulfur concentration may be thought to be proportional to time and the time axis in Fig. 1 may correspond to the c_t axis in Figs. 5 and 6–8(a). Although Fig. 1 has long been postulated, no direct observations of such a curve have been made experimentally or by simulations. The curves shown in Figs. 5 and 6–8(a) were the first simulation results that bear the resemblance of Fig. 1.

To examine the relationship between the peak in the c_e versus c_t observed in the simulations and that in the curve shown in Fig. 1, we have also performed simulations with gradual monomer addition. Experimentally, gradual monomer addition may be realized by adding the monomers drop by drop or by slow release by chemical reactions such as that described in Ref. [1]. The resultant monomer concentration versus t with a feeding rate of 5 monomers per 20τ was summarized in Fig. 11 where t denotes the time. The final total monomer concentration was 0.123 and $E=3k_BT$. Notice that similar to Fig. 1, the curve shown in Fig. 11 exhibited a peak in monomer concentration versus t. Note that the present simulation model is the first to generate a peaked solute concentration versus time as first proposed by LaMer and Dinegar. The main reason that the present model can generate such peaked solute concentration versus time during nucleation and growth of particles is that it allows both aggregation and dissolution. With gradual addition, the total concentration increases with time. For a given t, the corresponding c_t is also labeled at the top of Fig. 11. Clearly, the peak in monomer concentration versus t directly translates into a peak in c_e versus the corresponding total monomer concentration c_t. Indeed, the peak in c_e versus c_t can manifest as a peak in c_e versus t with gradual addition of monomers. However, the degree of supersaturation can vary with the feeding rate. The effect of the feeding rate on the degree of supersaturation is summarized in Figs. 12(a) and 12(b) where monomer concentration versus t and monomer concentration versus the corresponding c_t are plotted for various feeding rates, respectively. Note that the supersaturation peak became more prominent as the feeding rate was increased.

IV. CONCLUSION

We have examined the nucleation and growth process of colloidal particles using a reversible aggregation model (SAK model) with Monte Carlo simulations in two dimensions. The cluster-cluster aggregation mechanism, the prevalent aggregation mechanism in colloids, was the main aggregation mechanism in the model that allowed particles to nucleate and form. The monomer-unbinding process allowed dissolution to occur as well as particles to restructure and densify. Specifically, we examined the effect of the initial monomer concentration and that of the monomer-monomer attraction energy on the nucleation and growth of colloidal particles over a wide range of solution conditions. We showed that the equilibrium monomer concentration in solution c_e exhibited a peak with respect to the initial monomer concentration c_t and the solution may be divided in three regimes with respect to c_t. In the first regime where the initial monomer concentration was low, the solutions were below the solubility limit. All the monomers remained as individual monomers in the solution and the equilibrium monomer concentration increased linearly with the initial monomer concentration. In the second regime where the solution was supersaturated, small clusters of monomers began to occur while the equilibrium monomer concentration underwent a peak with respect to the initial monomer concentration. In the third regime, large particles form and the equilibrium monomer concentration slowly decreased with the initial monomer concentration. Moreover, the onset of nucleation regime, i.e., the second regime, occurred at a lower c_t

while the peak in c_e decreased with increasing monomer-monomer attraction energy (i.e., reduced solubility). The peak exhibited in the equilibrium monomer concentration versus the initial monomer concentration was manifested as a peak in the monomer concentration in solution with respect to time when monomers were gradually added to the solution and the peak height was enhanced by an increasing feeding rate. That the solute concentration peaks with respect to time during the nucleation and growth of colloidal particles where the solute is constantly fed to the solution has long been proposed by LaMer and Dinegar. The present simulations were the first to illustrate such behavior. The reason that the present model can generate such peaked solute concentration versus time is that it allows both aggregation and dissolution. We further showed that the supersaturation peak with time decreased and eventually diminished as the feeding rate decreased. The equilibrium monomer concentration surrounding a particle was shown to follow the Kelvin equation with respect to particle size, further indicating that the present model also captured the correct physics of a solution in its final regime of nucleation and growth.

ACKNOWLEDGMENT

This work was supported by a grant from the National Science Foundation, Grant No. DMR-9712773.

[1] V. K. LaMer and R. H. Dinegar, J. Am. Chem. Soc. **72**, 4847 (1950).
[2] J. Liu, M. Sarikaya, W. Y. Shih, W.-H. Shih, and I. A. Aksay, in *Fractal Aspect of Materials*, edited by J. H. Kaufman, J. Martin, and P. W. Schmidt, Mater. Res. Soc. Symp. Proc. No. EA-20 (Materials Research Society, Pittsburgh, 1989), p. 147.
[3] J. J. Murphy, A. M. Posner, and J. P. Quirk, J. Colloid Interface Sci. **56**, 270 (1976); **56**, 284 (1976); **56**, 298 (1976); **56**, 312 (1976).
[4] J. H. A. Van der Woude and P. L. deBruyn, Colloids Surf., A **11**, 391 (1983).
[5] E. Santacesaria, M. Tonell, G. Storti, R. C. Pace, and S. Carra, J. Colloid Interface Sci. **111**, 44 (1986).
[6] N. Uyeda, M. Nishino, and E. Soito, J. Colloid Interface Sci. **43**, 264 (1973).
[7] G. H. Bogush and C. F. Zukoski, J. Colloid Interface Sci. **142**, 19 (1991).
[8] W. Stober, A. Fink, and E. Bohn, J. Colloid Interface Sci. **26**, 62 (1968).
[9] W. Y. Shih, I. A. Aksay, and R. Kikuchi, Phys. Rev. A **36**, 5015 (1987).
[10] W. Y. Shih, J. Liu, W.-H. Shih, and I. A. Aksay, J. Stat. Phys. **62**, 961 (1991).
[11] J. Liu, M. Sarikaya, W. Y. Shih, and I. A. Aksay, Phys. Rev. A **41**, 3206 (1990).
[12] P. Meakin, Phys. Rev. Lett. **51**, 1119 (1983).
[13] M. Kolb, R. Botet, and R. Jullien, Phys. Rev. Lett. **51**, 1123 (1983).
[14] W. Y. Shih, W.-H. Shih, and I. A. Aksay, in *Physical Phenomena in Graduate Materials*, edited by G. D. Cady, T. H. Geballe, and P. Sheng, Mater. Res. Soc. Symp. Proc. No. 195 (Materials Research Society, Pittsburgh, 1990), p. 477.
[15] T. Terao and T. Nakayama, J. Phys.: Condens. Matter **11**, 7071 (1999).
[16] J. Liu, W. Y. Shih, R. Kikuchi, and I. A. Aksay, J. Colloid Interface Sci. **142**, 369 (1991).
[17] M. Yasrebi, W. Y. Shih, and I. A. Aksay, J. Colloid Interface Sci. **142**, 357 (1991).
[18] W. Y. Shih, W. H. Shih, and I. A. Aksay, J. Am. Chem. Soc. **79**, 2587 (1996).
[19] D. A. Weitz, and M. Olivera, Phys. Rev. Lett. **52**, 1433 (1984).
[20] C.-Y. Yang and W.-H. Shih, J. Am. Chem. Soc. **82**, 436 (1999).
[21] W. Y. Shih, J. P. Hirth, and D. Stroud, Phys. Rev. B **34**, 2895 (1986).